





ORIGINAL ARTICLE

Varying the sustained release of BMP-2 from chitosan nanogel-functionalized polycaprolactone fiber mats by different polycaprolactone surface modifications

Julius Sundermann¹  | Sarah Oehmichen² | Steffen Sydow² |
 Laura Burmeister^{3,4} | Bastian Quaas⁵ | Robert Hänsch^{6,7}  | Ursula Rinas^{5,8}  |
 Andrea Hoffmann^{3,4} | Henning Menzel²  | Heike Bunjes¹

¹Technische Universität Braunschweig, Institut für Pharmazeutische Technologie und Biopharmazie, Braunschweig, Germany

²Technische Universität Braunschweig, Institut für Technische Chemie, Braunschweig, Germany

³Niedersächsisches Zentrum für Biomedizintechnik, Implantatforschung und Entwicklung (NIFE), Hannover, Germany

⁴Medizinische Hochschule Hannover (MHH), Labor für Biomechanik und Biomaterialien, Orthopädische Klinik, Gradierete Implantate und Regenerative Strategien im Skelettsystem, Hannover, Germany

⁵Leibniz Universität Hannover, Institut für Technische Chemie, Hannover, Germany

⁶Technische Universität Braunschweig, Institut für Pflanzenbiologie, Braunschweig, Germany

⁷Center of Molecular Ecophysiology (CMEP), College of Resources and Environment, Southwest University, Chongqing, China

⁸Helmholtz-Zentrum für Infektionsforschung, Braunschweig, Germany

Correspondence

Heike Bunjes, Institut für Pharmazeutische Technologie, Technische Universität Braunschweig, Mendelssohnstraße 1, D-38106 Braunschweig, Germany.
 Email: heike.bunjes@tu-braunschweig.de

Funding information

Deutsche Forschungsgemeinschaft, Grant/Award Number: FOR 2180; Niedersächsisches Ministerium für Wissenschaft und Kultur

Abstract

Polycaprolactone (PCL) fiber mats with different surface modifications were functionalized with a chitosan nanogel coating to attach the growth factor human bone morphogenetic protein 2 (BMP-2). Three different hydrophilic surface modifications were compared with regard to the binding and *in vitro* release of BMP-2. The type of surface modification and the specific surface area derived from the fiber thickness had an important influence on the degree of protein loading. Coating the PCL fibers with polydopamine resulted in the binding of the largest BMP-2 quantity per surface area. However, most of the binding was irreversible over the investigated period of time, causing a low release *in vitro*. PCL fiber mats with a chitosan-graft-PCL coating and an additional alginate layer, as well as PCL fiber mats with an air plasma surface modification boundless BMP-2, but the immobilized protein could almost completely be released. With polydopamine and plasma modifications as well as with unmodified PCL, high amounts of BMP-2 could also be attached directly to the surface. Integration of BMP-2 into the chitosan nanogel functionalization considerably increased binding on all hydrophilized surfaces and resulted in a sustained release with an initial burst release of BMP-2 without detectable loss of bioactivity *in vitro*.

KEYWORDS

BMP-2, chitosan coating, growth factor delivery, PCL fiber scaffold, surface modification

[Correction added on 24 September 2020, after first online publication: Projekt Deal funding statement has been added.]

This is an open access article under the terms of the Creative Commons Attribution License, which permits use, distribution and reproduction in any medium, provided the original work is properly cited.

© 2020 The Authors. *Journal of Biomedical Materials Research Part A* published by Wiley Periodicals LLC.

1 | INTRODUCTION

The local application of cytokines, including growth factors, to stimulate regeneration processes in damaged tissue is a promising field of regenerative medicine. Critical tissue defects are currently mainly treated with autologous tissue transplants (Amini, Laurencin, & Nukavarapu, 2012). For the repair of defects for which no tissue-based scaffolds are available, such as complex tissue transitions, however, there are no clinical solutions so far. One approach to close this gap is to use natural or synthetic biomaterials that can provide the required properties of these tissue transitions. However, such artificial scaffolds lack the necessary bioactive triggers for directed tissue repair (Longo, Lamberti, Rizzello, Maffulli, & Denaro, 2012). The bone-inducing growth factor bone morphogenetic protein 2 (BMP-2), which is being investigated primarily for the repair of critical-sized bone defects, can also be used for the reconnection of the tendon to bone (Lee et al., 2016; Prabhath, Vernekar, Sanchez, & Laurencin, 2018). In order for recombinant human BMP-2 (rhBMP-2) to fulfill this purpose, it is crucial to precisely control the protein release at the target site, both spatially and temporally. Fast release resulting in high local doses can lead to ectopic bone growth and soft tissue inflammation (Shields et al., 2006). Moreover, BMP-2 has a short physiological half-life ($t_{1/2} = 0.3$ days [Ruhé et al., 2006]) and has to be constantly released over a period of several weeks in order to be effective (Yamamoto, Takahashi, & Tabata, 2003). A sustained release is therefore required, although a certain burst release has been shown to increase efficacy (Olthof et al., 2018). Because of its positive charge, a pronounced tendency to enter into hydrophobic interactions via its hydrophobic patches (Utesch, Daminelli, & Mroginski, 2011), and its affinity to glycosaminoglycans such as heparin or to domains like fibronectin type III (Martino et al., 2011), BMP-2 can be very efficiently bound to surfaces (Marquetti & Desai, 2018; Ruppert, Hoffmann, & Sebald, 1996). Simple surface attachment strategies do, however, not provide any mechanism for controlling the release. Bulk polymer release systems like matrices of polylactic-co-glycolic acid on the other hand may provide controlled release but cannot be easily coated on a nanoscale to a fine scaffold structure (Quinlan et al., 2015). To restore the tissue transition between bone and tendon, a scaffold structure is required in which growth factors can exert their stimulating effect on cell recruitment and growth. For this purpose, electrospun polycaprolactone (PCL) is a promising biodegradable and FDA-approved material to mimic the extracellular environment of tendon tissue. Limitations of biocompatibility as a result of the high hydrophobicity of PCL can be overcome by surface modifications (Gniesmer et al., 2019).

For example, chitosan-graft-PCL (CS-g-PCL) can be crystallized onto PCL fibers to introduce cationic amino groups (de Cassan et al., 2018). This results in scaffolds with a hydrophilic fiber surface, which showed an improved vascularization and a reduced tissue encapsulation compared to unmodified PCL *in vivo* (Gniesmer et al., 2019). Another way to obtain a more hydrophilic surface is through the use of polydopamine coatings. Self-polymerization of dopamine to polydopamine (PDA) occurs at a pH of pH 8.5. In contrast to the PCL graft, this coating creates a surface with a negative

surface charge over a wide pH range (Ryu, Messersmith, & Lee, 2018). A further option is the use of an air plasma treatment to introduce hydrophilic and negatively charged moieties to a polymeric surface (Desmet et al., 2009). All of these strategies are suitable to increase the biocompatibility of PCL. They also offer the possibility of utilizing ionic interactions for further surface functionalization.

An effective way of controlling drug release on virtually any charged surface is the use of polyelectrolyte coatings. Layer-by-Layer assembly, in which a charged substrate is alternately immersed in solutions of positively and negatively charged polymers to form a nanolayer thin film, has been investigated as a drug release concept for many types of surfaces (Boudou, Crouzier, Ren, Blin, & Picart, 2010; Costa & Mano, 2014; Jewell & Lynn, 2008). Films from chitosan (CS), which is known as a good substrate to create biomimetic properties (Drotleff et al., 2004), have already been used for the immobilization of BMP-2 (Abarrategi et al., 2009). By ionotropic gelation of CS with tripolyphosphate (TPP), gel-like CS-TPP nanoparticles (CS-TPP-NP) can be produced. When applied to a negatively charged surface the CS-TPP-NP fuse into a film. By prior application of a negatively charged polymer such as alginate, also positively charged surfaces can indirectly be used for the coating with CS-TPP-NP. The combination with additional negatively charged alginate layers alternating with CS layers can be used to produce controllable drug-releasing multilayer coatings (Sydow, de Cassan, et al., 2019).

The binding mode of the protein is an important criterion in determining whether surface modifications can be used to produce suitable coatings for controlled drug release. The type of modification of the PCL surface may have a decisive influence on whether the protein tends to bind directly to the surface or rather indirectly via incorporation into the forming CS matrix. The aim of this study was to test the influence of various PCL surface modifications associated with a CS-TPP-NP coating on the loading and release of BMP-2 from PCL fiber scaffolds.

2 | MATERIALS AND METHODS

2.1 | Polymers and other chemicals

Unless otherwise stated all chemicals, including PCL, CS ($M_n = 110,000$ – $150,000$ g/mol), and sodium alginate ($M/G = 1.3$) were purchased from Sigma-Aldrich, St. Louis, MO. Purified CS was obtained according to a method published by Gan et al. (Gan, Wang, Cochrane, & McCarron, 2005). Briefly, CS was mixed with sodium hydroxide solution (1 g of CS in 10 ml of 1 M sodium hydroxide) and stirred for 2 hr at 70°C. CS flakes were filtered off, washed with deionized water, and were dissolved in 1% (wt/vol) acetic acid. The degree of acetylation (DA) was determined to 17% via ^1H NMR spectroscopy.

2.2 | PCL fiber mats

The PCL fiber mats were electrospun from a PCL ($M_n = 80,000$ g/mol) solution of 17 wt% in 2,2,2-trifluoroethanol at the Institute for

Multiphase Processes at the Leibniz University of Hanover, Germany, according to an optimized electrospinning method described before (de Cassan et al., 2018). The electrospun source fiber mats that are hereinafter referred to as "batch fiber mats", had a size of $\sim 50 \times 5$ cm and a thickness of about 0.33 mm. A total of four different batch fiber mats (batch N° 1–4) were used in this study.

The mass-specific surface areas (S_m) of the batch fiber mats N° 1–3 were calculated from the mean fiber diameters (d), measured by light microscopy. Fibers were examined at random locations on both sides of the fiber mats. As a result of the high length to thickness ratio of the individual fibers, the cross-sectional fiber surface area is negligibly small compared to the lateral surface area. For the calculation of S_m , the fiber mat was therefore considered as a PCL cylinder without bases. The density (ρ) of the PCL used was 1.145 g/cm³ (Sigma-Aldrich, 2018).

S_m is given by:

$$S_m = \frac{S_{\text{cylinder}}}{V_{\text{cylinder}} \rho} = \frac{\pi d l^2}{\pi d^2 l \rho} = \frac{4}{d \rho}$$

2.3 | Production, refolding, and purification of non-glycosylated rhBMP-2

Preparation, refolding, and purification of dimeric non-glycosylated rhBMP-2 was performed by refolding of rhBMP-2 from inclusion bodies (IBs) produced in *Escherchia coli* and subsequent purification as previously described (Quaas et al., 2019).

The final, refolded and chromatographically purified rhBMP-2 dimer (simply referred to as BMP-2 in the following) was dialyzed against 50 mM 2-(N-morpholino) ethanesulfonic acid buffer (MES, pH 5) using a Zellultrans membrane with 6,000–8,000 MWCO (Carl Roth, Karlsruhe, Germany). The dialysate was filtered with a 0.22 μ m polyethersulfone sterile filter (Sartorius, Göttingen, Germany) and the filtrate with a final concentration of 0.132 mg/ml was stored at -80°C .

2.4 | Fluorescence labeling of BMP-2 (Cy3-BMP-2)

BMP-2 (0.5 mg/ml) was labeled according to the slightly modified manufacturer's protocol of the Amersham Cy3 Mono-Reactive Dye labeling kit (GE Healthcare, Chicago, IL, code: 25–8,009-86). Because of the poor solubility of BMP-2 at pH 7.4, 3-(N-morpholino) propanesulfonic acid (MOPS) pH 6.5 was used as a separation buffer instead of phosphate-buffered saline (PBS). Separation of protein from the free dye with a Bio-Gel P-10 column (BioRad, Hercules, CA) was performed after an additional dialysis step using a Zellultrans membrane with 6,000–8,000 MWCO (Carl Roth, Karlsruhe, Germany) against 1 mM HCl. Cy3-BMP-2 with a final concentration of 0.102 mg/ml (determined UV-metrically at 280 nm [NanoDrop 1000, Thermo Fisher, Waltham, MA]) was stored at -80°C .

2.5 | CS-g-PCL-Alg coating of PCL fiber mats

Chitosan-graft-PCL (CS-g-PCL) copolymer was synthesized and coated onto the batch fiber mats N° 1 and 2 to generate a positively charged surface as previously described by de Cassan et al. (2018). The CS-g-PCL coated batch fiber mats were additionally coated with an alginate layer (CS-g-PCL-Alg) to obtain a negative surface charge by dipping into an aqueous solution of sodium alginate (5 mg/ml) for 10 min. Subsequently, the batch fiber mats were rinsed several times with deionized water and vacuum-dried for 24 hr at room temperature.

2.6 | Polydopamine coating of PCL fiber mats

Sections of the batch fiber mat N° 3 with a size of 8×16 mm were immersed in a solution of 1 mg/ml dopamine hydrochloride in a mixture of Tris buffer (0.01 M, pH = 8.5) and ethanol (80/20 vol/vol) for 24 hr under shaking at room temperature. The fiber mat sections were then rinsed 10 times for 5 min with ultrapure water and dried under vacuum until their weight remained constant.

2.7 | Air plasma treatment of PCL fiber mats

Plasma surface modification was performed in the vacuum chamber of a MiniFlecto® plasma system (plasma technology GmbH, Herrenberg, Germany) using sections of the batch fiber mat N° 3 with a size of 8×16 mm. After the evacuation of the chamber, a pressure of 0.1 mbar was set by a controlled inflow of air. A power of 30 W for 60 s was used for the subsequent plasma treatment. The modification under these conditions took place twice to treat both sides of the fiber mat sections.

2.8 | Preparation of fiber mat samples

For all loading and release experiments fiber mat sections of 8×16 mm (fiber mat samples) were used. The fiber mat samples were cut out of the batch fiber mats using scalpel and scissors. Because of the decreasing thickness toward the sides of the batch fiber mats, only the central area of $\sim 50 \times 3.2$ cm was used for sample cutting. In order to determine the usable area and to exclude possible defects, the batch fiber mats were assessed using densitometric transillumination images taken with a gel documentation system (Supporting Information Section 1, Figure S1).

The differently modified PCL fiber mat samples were used as substrates for loading and release experiments. In the following, fiber mat samples with various surface modifications are referred to as fiber mat variants. A summary of the fiber mat variants is given in Figure 1. The mass of the fiber mat samples was determined using a microbalance (XS3DU, Mettler Toledo, Greifensee, Switzerland).

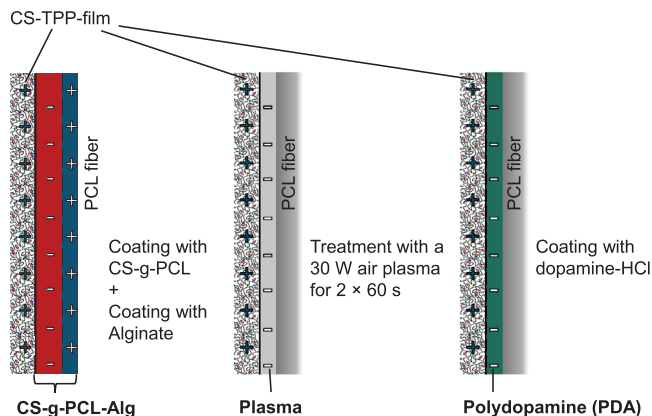


FIGURE 1 Schematic of investigated fiber mat variants

2.9 | Surface zeta potential measurement of fiber mat variants

The surface zeta potential of the fiber mat variants in the pH range from pH 2 to pH 9.5 was determined using the SurPASS™ 3 Electrokinetic Analyzer (Anton Paar GmbH, Austria). For each measurement, two 1 × 2 cm fiber mat cut pieces were glued to the two-sample holders of the adjustable gap cell using adhesive tape. One hundred milliliters of 10 mM KCl was passed through the set gap width of approximately 100 μm with a pressure ramp of 600–200 mbar. Titration with HCl (0.05 M) and KOH (0.05 M) for pH adjustment was carried out automatically.

2.10 | Preparation of CS-TPPnanoparticles

In order to obtain CS with the desired solubility properties, the DA was adjusted. The general procedure of CS acetylation and nanoparticle preparation was published previously (Poth, Seiffart, Gross, Menzel, & Dempwolf, 2015). Briefly, purified CS with a DA of 17% was dissolved in 1% (vol/vol) acetic acid to get a concentration of 5 mg/ml. After volumetric doubling with ethanol, acetic acid anhydride was added to the reaction mixture in an amount calculated according to Freier, Koh, Kazazian, and Shoichet (2005). The mixture was stirred for 18 hr at room temperature. After subsequent dialysis against deionized water, the acetylated CS was lyophilized. The DA was calculated from ¹HNMR spectra as 42%.

For particle preparation, the acetylated CS was dissolved in 0.1% (vol/vol) acetic acid at a concentration of 1 mg/ml. Tripolyphosphate (TPP) was dissolved in deionized water at the same concentration. The TPP solution was rapidly mixed with the CS solution in a CS-TPP ratio of 3:1, which in previous studies reproducibly resulted in nanoparticles with a z-average diameter in the range of 143 ± 2 nm and a zeta potential of about 27 ± 1 mV (Sydow, de Cassan, et al., 2019).

For BMP-2-containing nanoparticle suspensions, 100 μl of 0.132 mg/ml BMP-2 in 50 mM MES buffer (pH 5) was added to 900 μL CS solution before mixing with TPP to obtain 1 ml of nanoparticle suspension with a BMP-2 concentration of 13.2 μg/ml.

2.11 | Fluorimetric quantification of Cy3-BMP-2

The concentration of Cy3-BMP-2 was determined fluorometrically at 550 nm excitation and 605 nm emission in polypropylene 96/V well plates (Eppendorf AG, Hamburg, Germany, No. 0030601.904) with an Infinite® 200 pro plate reader (Tecan Ltd., Mänedorf, Zürich, Switzerland). Concentration series of Cy3-BMP-2 and blanks were measured in the corresponding sample medium. Cy3-BMP-2 concentration series and blanks in the 1 mg/ml CS-TPP-NP suspension were used as calibration for measurements of samples in CS-TPP-NP suspensions.

2.12 | Cy3-BMP-2 loading experiments on CS-g-PCL-Alg fiber mat variants

Stacks of either four or six fiber mat samples from batch N° 1 or 2 with defined masses were incubated in Cy3-BMP-2-containing suspensions of CS-TPP-NP, which had been prepared as described above (cf. 2.10), replacing BMP-2 by Cy3-BMP-2. The Cy3-BMP-2 concentration in the loading solution was 10.2 μg/ml. In addition, a loading experiment was carried out in which four fiber mat samples from batch N° 2 were incubated in 50 mM MES buffer pH 5 with 10.2 mg/ml Cy3-BMP-2 without the addition of CS-TPP-NP. All loading experiments were performed in 2 ml Low-Binding polypropylene tubes (Sorenson BioScience, Salt Lake City, USA, Cat# 12180).

During the loading experiments, the Cy3-BMP-2 concentration in the nanoparticle suspension was quantified fluorometrically at specified times over a period of 15, 23, or 30 min.

For each measurement, 100 μl of the suspension of Cy3-BMP-2-containing CS-TPP-NP were temporarily withdrawn from the loading tubes to black polypropylene 96/V well plates (Eppendorf AG, Hamburg, Germany, No. 0030601.904) and completely transferred back again after the measurement. The fiber mat samples remained in the Cy3-BMP-2-containing CS-TPP-NP suspension throughout the entire experiment. Quantification was performed during the immersion of the fiber mat samples. The amount of bound Cy3-BMP-2 was indirectly determined by the decrease in Cy3-BMP-2-concentration. At the end of the loading experiment, the fiber mat samples loaded with Cy3-BMP-2 were washed in deionized water for 2 min, dried under vacuum, and were kept dry at –20°C for one to 3 months until the start of release studies.

2.13 | Cy3-BMP-2 loading experiments on PDA and plasma mat variants

The procedure was the same as described above (cf. 2.12), with the difference that four fiber mats samples from the batch fiber mat N° 3 were used for all loading experiments. Experiments were carried out over a period of 60 min. The loaded fiber mat samples were stored for 1 week at –20°C in the dried state prior to the start of release studies.

2.14 | BMP-2 loading on polydopamine, plasma, and unmodified fiber mat variants without CS-TPP-NP

Four fiber mat samples each from the batch fiber mat N° 4 were incubated for 15 min in a 50 mM MES buffer containing 13.2 µg/ml unlabeled BMP-2 for 15 min. The BMP-2 loading of the fiber mat samples was determined by the protein concentration decrease in the loading solution quantified by an assay of BMP-2 biological activity (BRE-Luc-Assay, cf. 2.15).

BMP-2 loading without CS-TPP-NP was also carried out with the hydrophobic, unmodified PCL fiber mat samples. The immersion of the unmodified PCL fiber mat samples took place very slowly, following the slow absorption of the liquid into the pores of the fiber scaffolds. The slow immersion procedure ensured that a single liquid front was formed, preventing air inclusions and achieving complete wetting of the fiber mat samples.

2.15 | Quantification of BMP-2 activity by BRE-Luc assay

The BMP Responsive Element Luciferase (BRE Luc) Assay was essentially conducted as previously described (Lorenz et al., 2011). A mouse muscle satellite cell line C2C12 was stably transfected with the BRE firefly luciferase reporter plasmid containing an inhibitor of the differentiation promoter-luciferase construct from Korchynsky et al. (Korchynskyi & ten Dijke, 2002). For the quantification of BMP-2 activity in loading solutions (cf. 3.5), the assay was performed in a 96 well-plate format as described in (Quaas et al., 2019) and for the quantification of BMP-2 activity after release (cf. 3.4) in a 24 well-plate format as described in (Quaas et al., 2018).

2.16 | Quantification of BMP-2 by enzyme-linked immunosorbent assay (ELISA)

A commercial BMP-2 ELISA (BMP-2 TMB ELISA Development Kit, Peprotech Inc., Rocky Hill, NJ) was used according to the manufacturer's protocol with slight modifications. BMP-2 from own production (cf. 2.3) was used as a standard for the concentration calculation. The measurement was performed with an Infinite® 200 pro plate reader (Tecan Ltd., Mänedorf, Zürich, Switzerland). Standard curves were fitted with OriginPro 2015 (Origin® Labs, Northampton, MA) using a 4PL-logistic curve fit.

2.17 | *In vitro* BMP-2 release

Release experiments were performed in 1 ml of Peprotech ELISA diluent consisting of Dulbecco's PBS with 0.1% bovine serum albumin and 0.05% Tween 20 (part of TMB ELISA Buffer Kit, Catalog Number 900-T00, Peprotech Inc.) with an addition of 0.02% (wt/vol) sodium azide to prevent microbial growth (S8032, Sigma-Aldrich, St. Louis,

MO). Release experiments with subsequent activity determination in the BRE-Luc assay were performed without the addition of sodium azide. Fiber mat samples were incubated at 37°C inside of 2 ml polypropylene Low-Binding Tubes (Sorenson BioScience, Salt Lake City, UT, Cat# 12180) without agitation. Sampling was performed at specified points in time over a period of four to 8 weeks. At each sampling time, fiber mat samples were removed from the tubes, blotted against clean paper towels to remove the excess medium, and transferred to fresh release media. After removing the fiber mat samples, the tubes with the released BMP-2 were stored at 4°C until quantification of released protein by ELISA, BRE-Luc assay, or by fluorescence intensity measurements.

2.18 | Confocal laser scanning microscopy

Measurements were performed on a confocal laser scanning microscope cLSM-510META connected to the Axiovert 200 M (Carl Zeiss, Göttingen, Germany). The specimens were examined using the C-Apochromat 40×/1.2 water immersion objective. Excitation was performed with the 543 nm Helium laser. The emitted light was detected with the BP filter at 560–615 nm. Samples were measured in various depths and multiple times to verify the results.

3 | RESULTS

3.1 | Evaluation of fiber mat weight and surface area

The individual batch fiber mats had a very homogeneous fiber thickness over the entire surface (data not shown). Between the individual batch fiber mats, which were produced on different days, there were differences in the mean fiber diameter, which had a strong influence on the calculated mass-specific surface area (Figure 2). The larger fiber diameters of the batch fiber mat N° 2 and 3 compared to the batch fiber mat N° 1 resulted in a decreased mass-specific surface area. All fiber mat samples had weights between 7.4 and 7.8 mg per cm² of the macroscopic fiber mat surface.

3.2 | Zeta potential of fiber mat variants

All surface modifications led to a strongly increased surface charge compared to unmodified PCL (Figure 3). In order to evaluate the loading and release results, it is useful to consider the zeta potentials at the neutral pH of the release medium, as well as at the slightly acidic pH of the loading solutions.

At pH 7.4 all surfaces were negatively charged. The plasma variants showed the highest negative zeta potential at pH 7.4 of approximately –94 mV, while CS-g-PCL-Alg and PDA variants had a similar net charge of about –48 mV. In the slightly acidic pH range, there was a charge reversal on the PDA surface (~pH 4.5), while the CS-g-PCL-

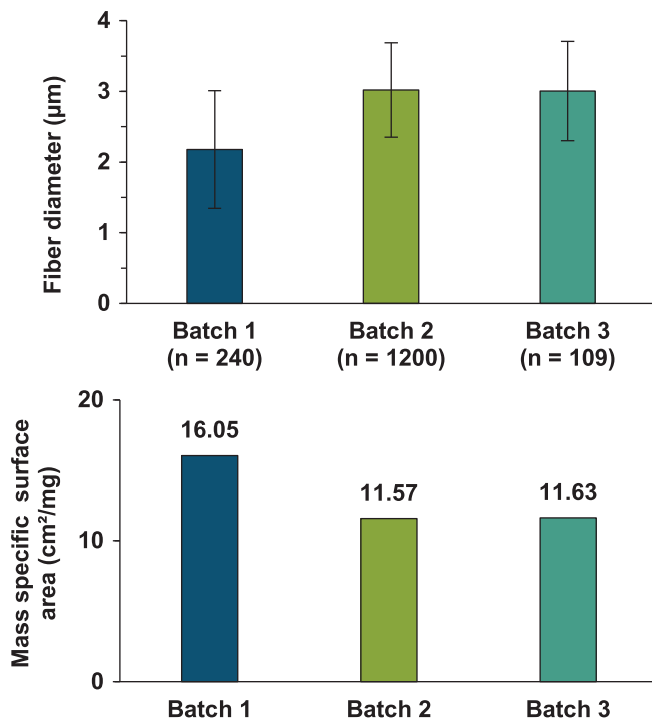


FIGURE 2 Mean fiber diameter and calculated approximate mass-specific surface area of the three fiber mat batches. Error bars indicate SD

Alg and the plasma variants exhibited a negative charge over the entire pH range tested. The absolute zeta potentials at pH 5 were in the order Plasma > CS-g-PCL-Alg > PDA > unmodified PCL.

3.3 | Cy3-BMP-2 loading on and release from different fiber mat variants using the CS-TPP-NP coating

According to literature, release studies with BMP-2 are associated with experimental challenges. Release and loading experiments with unlabeled BMP-2 in PBS, which are essentially limited to ELISA for quantification, showed inconsistencies such as fluctuating BMP-2 concentrations (Xia et al., 2018) or a very low BMP-2 release in relation to the loading quantity. Some authors have reported differing BMP-2 release rates in PBS compared to cell culture medium or serum (Ruhé et al., 2006; Strobel, Bormann, Kadow-Romacker, Schmidmaier, & Wildemann, 2011). BMP-2 has an isoelectric point of 8.5 (Uludag, D'Augusta, Palmer, Timony, & Wozney, 1999) and its solubility is extraordinarily dependent on ionic strength and pH (Quaas et al., 2019). Given the extremely poor solubility of BMP-2 in PBS-based buffers, there is a risk of release results being influenced by solubility- and aggregation-dependent recovery effects. In order to avoid this possible source of bias all quantitative experiments in which potentially interfering compounds such as CS were present were performed with Cy3-fluorescence-labeled BMP-2 in this study. Because BMP-2 is extremely prone to detrimental effects upon freezing and

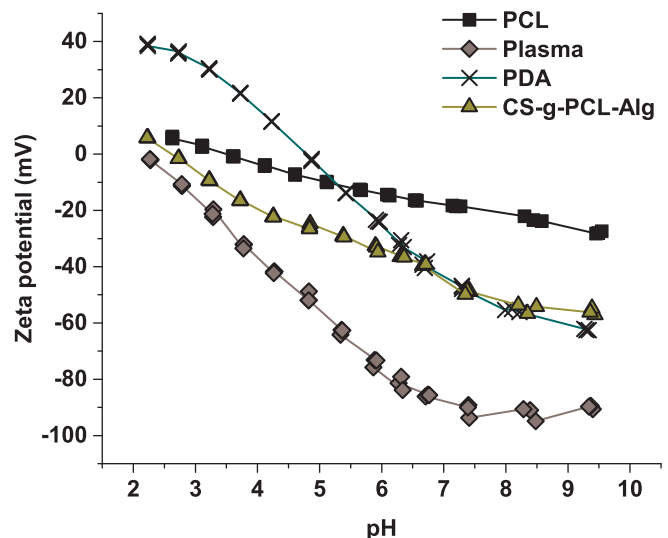


FIGURE 3 Evolution of zeta potential on the surface of the fiber mat variants in 10 mM KCl as a function of pH

thawing in the release buffer (Lochmann, Nitzsche, von Einem, Schwarz, & Mäder, 2010), release samples were not frozen but stored at 4°C until quantification.

The loading of the fiber mat samples was indirectly determined by monitoring the decrease of the Cy3-BMP-2 quantity in the loading dispersion. The loading experiment with CS-g-PCL-Alg fiber mat variants was carried out three times (referred to as L1, L2, and L3) with different numbers of fiber mat samples from the batch fiber mat N° 1 and 2 with different total surface areas (Table 1, more details in Supporting Information, Section 2, Table S1).

The decrease of the protein concentration in the loading dispersion depended on the total mass and surface area of the fiber mat samples used. In the case of the fiber mat samples from batch N° 1 (L1 and L2), the concentration in the loading solution had decreased to ~67% for 30 mg and to ~28% for 62 mg of fiber mat after 15 min (Figure 4a). The indirectly determined loaded amount of Cy3-BMP-2 was reflected by the Cy3-BMP-2 amount determined in the washing solutions, which was between 3.0 and 3.3% of the total loading (Figure 5).

Subtracting the Cy3-BMP-2 loss due to the washing step, this resulted in a Cy3-BMP-2 loading after 15 min of 115 (L1) and 113 ng (L2) per mg fiber mat. For the fiber mat samples from batch N° 2 (L3), there was only loading of 86 ng/mg fiber mat after 15 min. By comparing the bound Cy3-BMP-2 amount per fiber mat mass and per fiber surface area (Figure 4b,c), it can be seen that the bound quantity is more correlated with the fiber surface area than with the mass of the fiber mats.

The mean bound amount of Cy3-BMP-2 per fiber surface of all three experiments after 15 min was 7.22 ± 0.20 ng per cm². In order to evaluate the uncertainty of the quantification method, at the last two time points of the loading experiment L3, measurements of $3 \times 100 \mu\text{l}$ and $6 \times 100 \mu\text{l}$ were carried out instead of the single measurement of $100 \mu\text{l}$. The error bars in Figure 4a-c indicate the SD of

TABLE 1 Summary of CS-g-PCL-Alg loading experiments

Attributes	Test designation		
	L1	L2	L3
Fiber mat origin (Batch N ^o)	1	1	2
Number of fiber mats	6	4	4
Total fiber mat mass (mg)	62	30 ^a	38
Total fiber surface area (cm ²)	995	482 ^a	439
Total loading duration (min)	15	30	23
Cy3-BMP loading per fiber surface after 15 min (ng/cm ²)	7.15	7.07	7.43

^aBecause 21% of the total fiber mat area used (38 mg) was not wetted, the total available mass and surface area were corrected (determination of wetted surface in Supporting Information, Section 3, Figure S3).

these measurements and thus provide an explanation for the fluctuations in the individual curves.

During release experiments over 70 days, the mats of experiment L2 released 141 ng of the bound 159 ng and those of L3 93.5 ng of the bound 94 ng Cy3-BMP-2 per mg fiber mat, corresponding to a recovery of ~89 and 99%, respectively (Figure 4d). The lower Cy3-BMP-2 recovery in experiment L2 compared to L3 may be due to longer storage of fiber mat samples before the release of L2 (3 months) compared to L3 (1 month), which may have led to a small loss of the Cy3-label fluorescence intensity.

During the release study with the fiber mat samples from loading experiment L1, microbial contaminations became evident. As the contamination seemed to have had a strong influence on the measured release curves the data obtained were not comparable with that of L2 and L3. However, an average total release of 81 ng/mg corresponding to 70% of loaded Cy3-BMP-2 was determined after 35 days (Supporting Information, Section 2, Figure S2).

In a separate experiment, the Cy3-BMP-2 binding per cm² fiber surface area over time with CS-TPP-NP in the loading solution was compared to loading without adding CS-TPP-NP (Figure 6). Without CS-TPP-NP, 1.75 ng/cm² were bound after 17 min, which is more than four times less than when using CS-TPP-NP.

Upon loading with CS-TPP-NP, the Cy3-BMP-2 binding per cm² overtime was strongly dependent on the type of surface modification (Figure 7). The by far highest Cy3-BMP-2 binding was found on the PDA-based coating. The Cy3-BMP-2 binding to the plasma-treated PCL surface was only about half as high as to the PDA fiber mat variants. The binding to the CS-g-PCL-Alg fiber mat variants was about three times lower compared to the PDA variants.

The *in vitro* release was highest from the CS-g-PCL-Alg and plasma variants. From these two variants, the Cy3-BMP-2 was almost completely released, while only a small fraction of the Cy3-BMP-2 was released from the PDA variants (Figure 8a, more details in Supporting Information, Section 2, Table S2). As a result of the high binding to the PDA, however, the absolute release per surface area was comparable with that of the CS-g-PCL-Alg variants (Figure 8b). Regarding the total amount released, the highest release was observed from the plasma variants.

The release rate of the CS-TPP-functionalized fiber mat samples during the second week of release was ~0.083 ng/cm²/day (CS-g-PCL-Alg), 0.108 ng/cm²/day (PDA) and 0.127 ng/cm²/day (plasma). The release rate decreased in a similar way for all variants to about 0.014 ng/cm²/day (CS-g-PCL-Alg), 0.022 ng/cm²/day (PDA), and 0.012 ng/cm²/day (plasma) in the seventh week of release. The PDA variants showed a slightly slower decrease in the release rate, which correlates with a large amount of unreleased protein.

The binding of Cy3-BMP-2 via coating with CS-TPP-NPs to the surface of the plasma and CS-g-PCL-Alg fiber mat variants was confirmed by CLSM (Figure 9). Fluorescence on PDA variants was very weak and only became visible at a highly increased gain (Supporting Information, Section 4, Figure S5). The relatively low fluorescence signal on the Cy3-BMP-2-loaded PDA variants might be a result of the strong fluorescence quenching ability of PDA toward a wide spectrum of fluorescent dyes (Qiang, Li, Li, Chen, & Xu, 2014). No fluorescence was detectable on unloaded fiber mat samples (data not shown).

3.4 | Quantification of BMP-2 biological activity after release from CS-TPP-coated CS-g-PCL-Alg fiber mat variants by BRE-Luc assay

According to the results of the BRE-Luc Assay, active BMP-2 was released from the fiber mats (Figure 10). However, during the first few days, the amount of BMP-2 released from CS-g-PCL-Alg variants appeared to be up to 10 times higher than the fluorometrically measured release of Cy3-BMP-2. In the second week of the release, both methods measured a BMP-2 release of about 6 ng/mg fiber mat within 5 days. According to results obtained in a different set of experiments, BMP-2 release results based on the BRE-Luc assay were affected by a complex interfering effect caused by dissolving CS. The interfering effect of CS resulted in a highly increased BMP-2 recovery in the BRE-Luc-Assay, as well as in ELISA during the first days of release and will be discussed in more detail elsewhere (manuscript in preparation). However, the BMP-2 activity determined by BRE-Luc assay after release did not indicate any loss of activity.

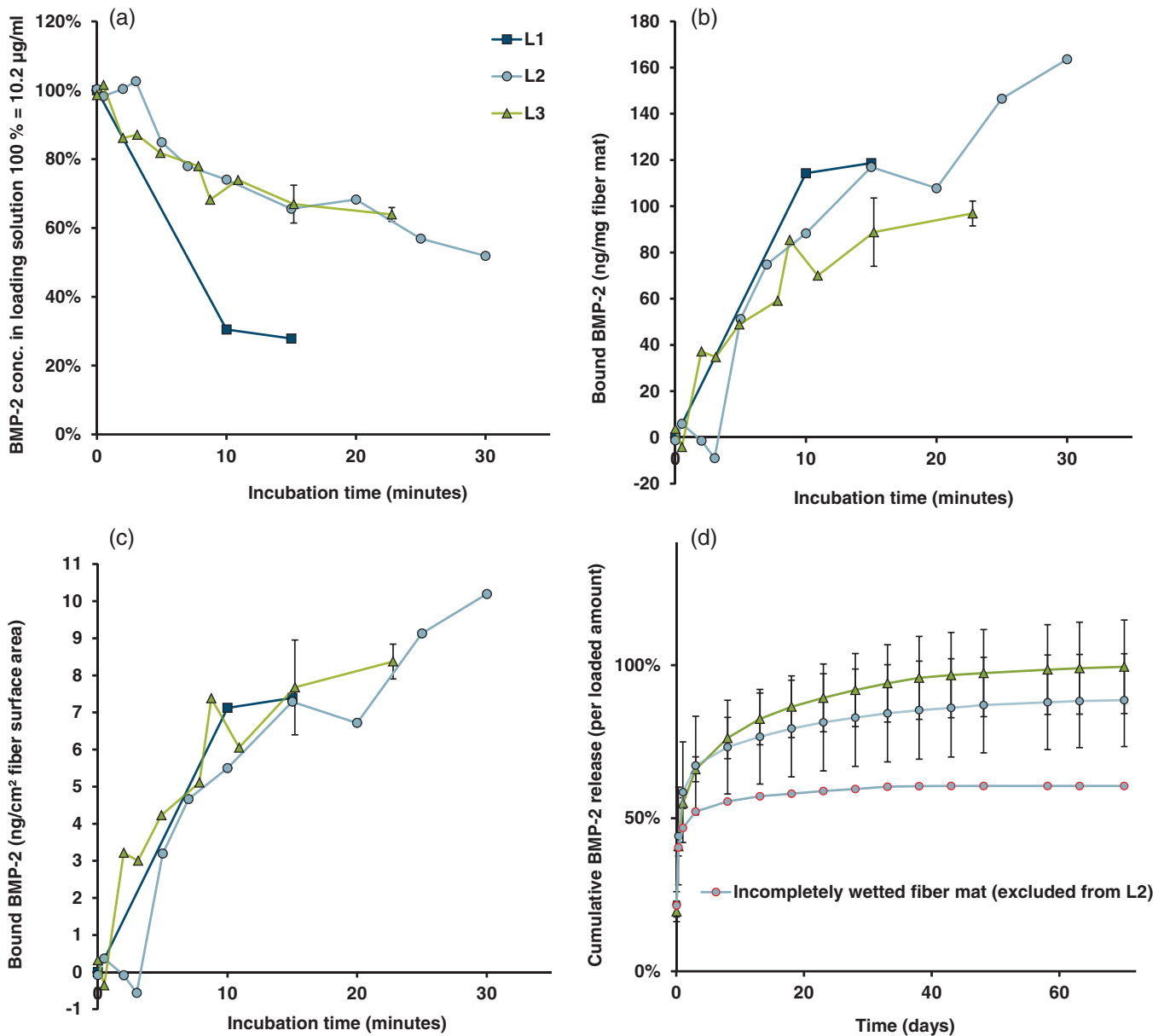


FIGURE 4 (a) Fluorometrically determined Cy3-BMP-2 concentration decay in the loading dispersion during the three loading experiments L1–L3. (b) Calculated bound Cy3-BMP-2 amount per mg fiber mat over time (c) Bound Cy3-BMP-2 amount per cm² of calculated fiber surface area over time. Error bars in (a), (b), (c) indicate SD between multiple measurements of the same solution ($n = 3$ –6), data points without error bars represent single measurements. (d) Mean cumulative Cy3-BMP-2 release ($n = 3$), error bars indicate SD between single release experiments (L1–L3)

3.5 | BMP-2 loading on and release from unmodified PCL, plasma, and PDA fiber mat variants without CS-TPP-NP

When loading the PDA, plasma, and unmodified PCL fiber mat samples from a plain MES buffered solution of 13.2 µg/ml BMP-2, an additional loading solution was prepared in which no mats were immersed as a negative control. A concentration of 13.2 µg/ml biologically active BMP-2 was observed in the control without fiber mats, indicating no decrease in concentration (Figure 11).

Loading to plasma variants was about 190 ng/mg and loading to PDA variants was about 143 ng/mg. The plasma variants had released a negligibly small amount of 5 ng/mg BMP-2 after 15 days (1.8%) (Figure 12). The BMP-2 release from the PDA variants was below the quantification limit of the ELISA. Apparently, the direct connection to the charged PDA and plasma surface led to a BMP-2 binding that was irreversible under the tested conditions.

The loading solution of the unmodified fiber mat samples still contained ≈ 5.16 µg/ml after loading. This corresponds to a total loading of ~ 268 ng/mg. During the release, about 89 ng/mg was released from the unmodified PCL mats, corresponding to a release of 33.4%.

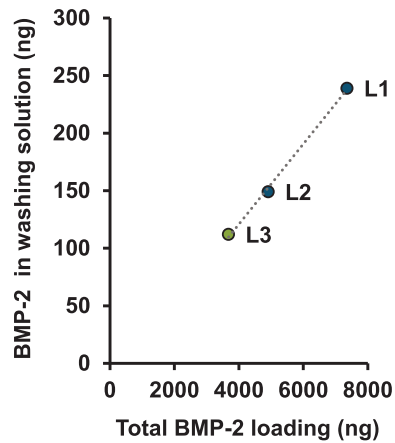


FIGURE 5 Correlation of the Cy3-BMP-2 quantity in the washing solutions and the quantity loaded to the fiber mats

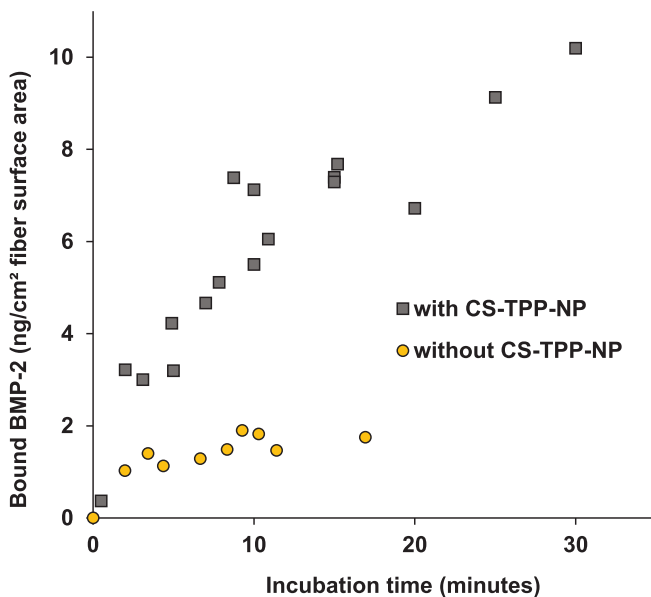


FIGURE 6 Bound Cy3-BMP-2 per cm² fiber surface area during loading on the CS-g-PCL-Alg fiber mat variants with and without the presence of CS-TPP-NP

However, because of the high hydrophobicity of the unmodified PCL, roughly about half of the fiber mat surface was not wetted during the release study (depicted in Supporting Information, Section 3, Figure S4). The incomplete release of the unmodified mats was, therefore, probably a result of incomplete wetting. In the release medium, the interfacial free energy is reduced by the addition of Tween 20, which was expected to lead to a reduction of hydrophobic interactions during the release study. In addition, superficially bound BMP-2 should be displaced from the surface by albumin in the release medium (Vroman effect) (Vroman & Adams, 1969). These two factors lead to the assumption that the bound BMP-2 could have been more or less completely released from the wetted areas of the unmodified PCL fiber mat samples. 98% of the total released quantity from the unmodified fiber mat samples was released during the first 5 days. In

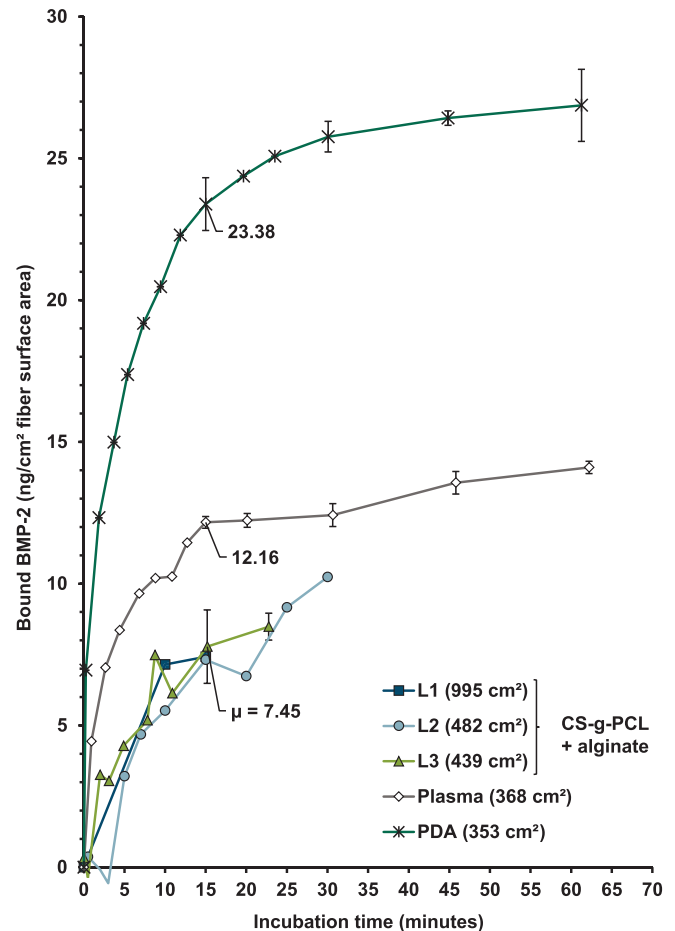


FIGURE 7 Cy3-BMP 2-loading per cm² of fiber surface area over time of all loading experiments (calculated fiber surface in brackets). Error bars indicate SD between multiple measurements of the same solutions ($n = 6$), data points without error bars represent single measurements, $\mu =$ mean of L1–L3. Data for L1–L3 from Figure 4c

contrast to the fiber mats with CS-TPP-NP functionalization (Figure 8), unmodified PCL showed practically no sustained BMP-2 release.

4 | DISCUSSION

4.1 | BMP-2 binding by direct surface adsorption

Proteins can bind to surfaces both via hydrophobic and ionic interactions (Rabe, Verdes, & Seeger, 2011). For surfaces with a wetting angle θ of more than 62.4°, protein binding can be explained by hydrophobic interactions (Vogler, 1998). It can, therefore, be assumed that the high BMP-2 binding to unmodified PCL fiber mats ($\theta \approx 124^\circ$ [de Cassan et al., 2018]) was largely due to hydrophobic interactions (Figure 11). Because of the strong hydrophilization by the surface modifications applied in the present study, protein binding can no longer occur via hydrophobic interactions on these surfaces and can, therefore, only be explained by ionic interactions (de Cassan et al., 2018). Surface modification by plasma treatment, which resulted in a higher negative surface charge than the PDA modification (Figure 3), led to a higher binding of the positively

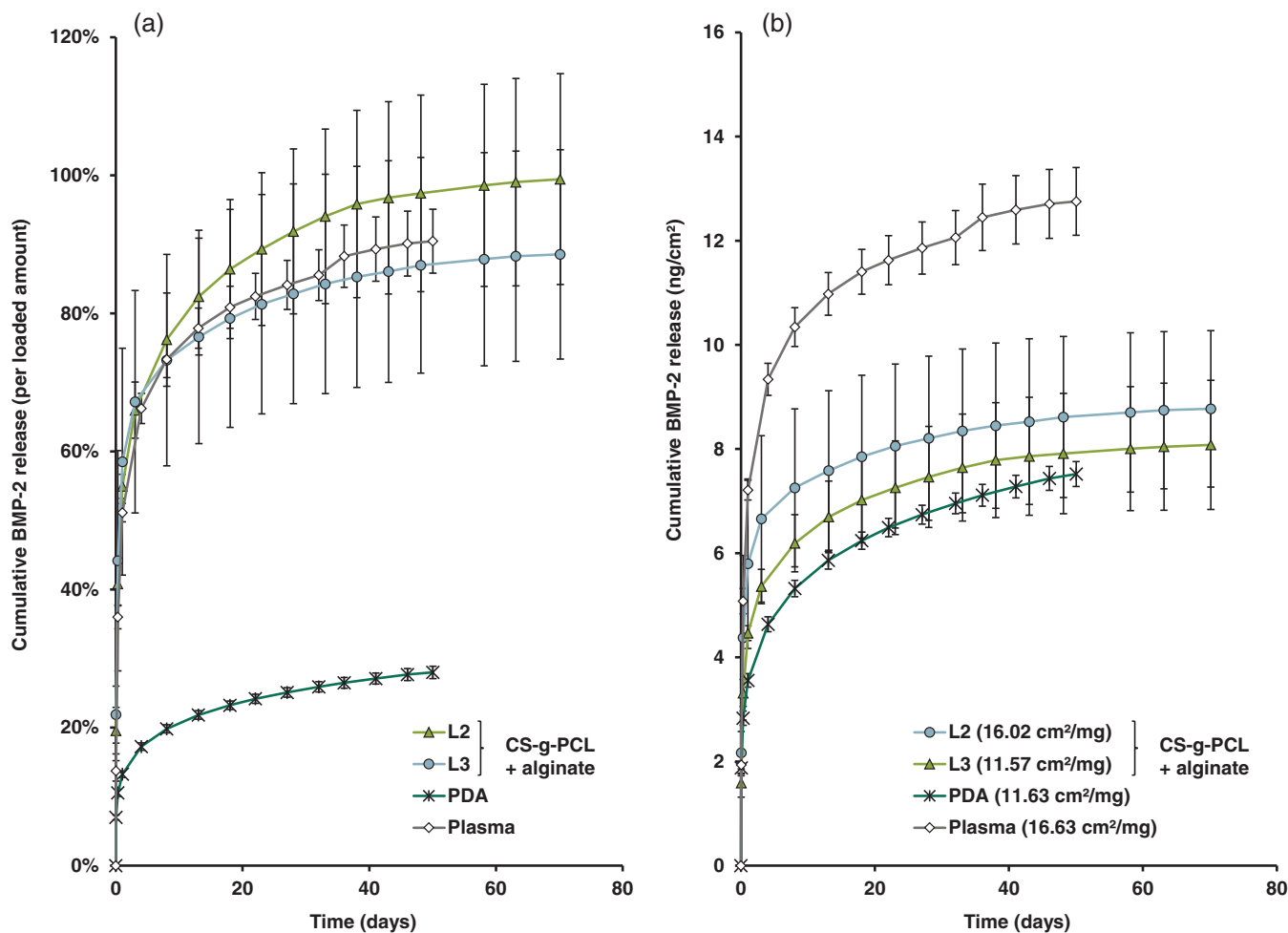
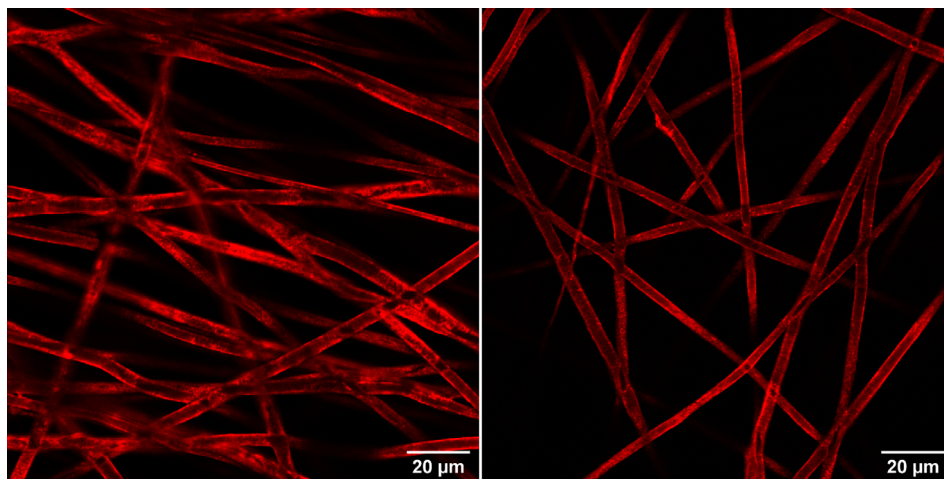


FIGURE 8 Mean cumulative Cy3-BMP-2 release on relative (a) and absolute (b) scale ($n = 3$), error bars indicate SD between single release experiments. Data in (a) for L2 and L3 from Figure 4d

FIGURE 9 CLSM images of fiber mat samples after Cy3-BMP-2 loading experiments using CS-TPP-NP (results are shown in Figure 7). Left: CS-g-PCL-Alg fiber mat variant from experiment L1. Right: Plasma variant. CLSM, confocal laser scanning microscope



charged BMP-2. Binding to the CS-g-PCL-Alg coating resulted in a much lower BMP-2 loading, possibly due to the gel-like character of the alginate surface. Interestingly, direct BMP-2 surface binding via hydrophobic interactions led to higher BMP-2 adsorption than all binding approaches via ionic interactions.

4.2 | BMP-2 binding and release using the CS-TPP-NP coating

By combining surface hydrophilization with the use of the CS-TPP-NP coating, considerable enhancement in protein binding was achieved

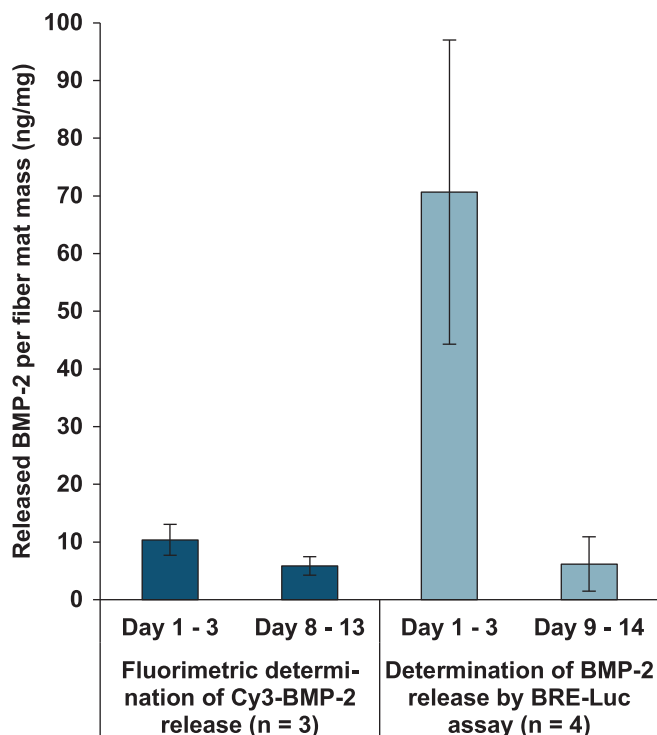


FIGURE 10 Comparison of the BMP-2 release of CS-g-PCL-Alg fiber mat variants determined by activity (BRE-Luc in 24 well-plates) and by fluorescence labeling. Error bars indicate SDs between single measurements ($n = 3$)

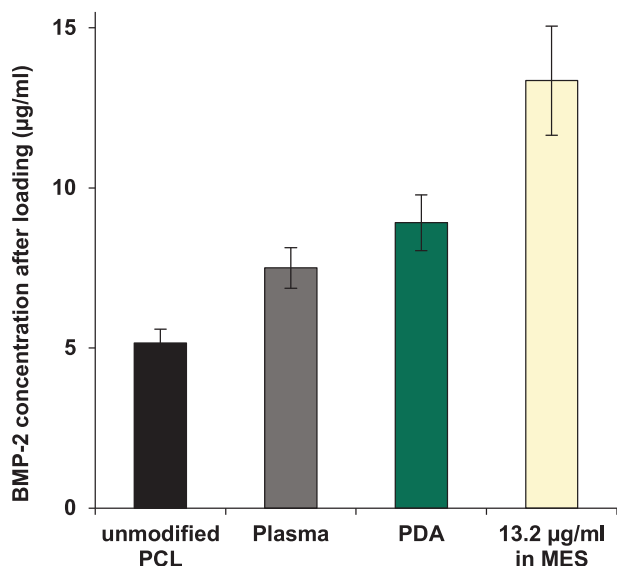


FIGURE 11 BMP-2 concentrations determined by BRE-Luc Assay (96 well-plates) before (13.2 $\mu\text{g/ml}$) and after 15 min incubation of differently modified PCL fiber mats in solutions of 13.2 $\mu\text{g/ml}$ BMP-2 in MES pH 5, error bars indicate SDs between single measurements ($n = 6$)

on all surface modifications (Figures 6, 7, and 11). Because of the higher BMP-2 loading from CS-TPP-NP dispersions (as compared to free BMP-2 in solution), it is unlikely that BMP-2 and CS-TPP adhere

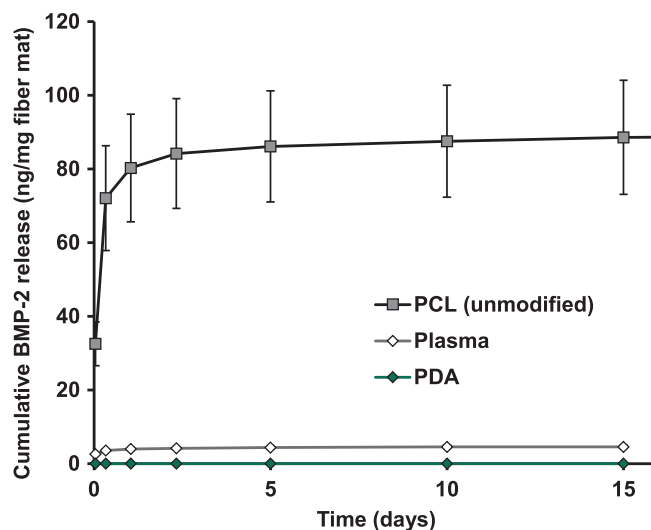


FIGURE 12 Cumulative BMP-2 release per mg fiber mat after loading of fiber mat samples without the use of CS-TPP-NP as measured by ELISA. Error bars indicate SDs between single measurements ($n = 3$). Substantial parts of the unmodified fiber mat samples were not wetted during the release study (Supporting Information, Section 3, Figure S4). The release results of the unmodified fiber mat variants, therefore, have only limited comparability (see text for details)

simultaneously but largely independently to the modified fiber mats. In this case, chitosan would enter into a competitive binding reaction with BMP-2 for free surface sites and the loading using the CS-TPP-NP would be expected to be lower than without CS-TPP-NP.

Although both BMP-2 and CS are positively charged, molecular dynamics simulations by Wang et al. showed an attractive interaction of these two substances, which depends on the degree of deacetylation of CS (Wang et al., 2019). Experimentally, a loading of CS particles with BMP-2 could only be shown for sulfated CS so far (Cao, Wang, Hou, Xing, & Liu, 2014), which is to be expected because of the known interaction of BMP-2 with sulfated glycosaminoglycans such as heparin. It is possible that BMP-2, together with TPP, is deposited in the negatively charged cores of the positively charged CS-TPP-NP during the ionotropic gelation of the nanoparticles (Poth et al., 2015). According to this theory, BMP-2 would be carried by the CS-TPP-NP onto the fiber mats, which would explain the increased BMP-2 loading.

BMP-2 is known for direct and partially covalent binding to PDA coatings (Cho et al., 2014; Lee, Lee, & Heo, 2018; Zhao et al., 2017). The covalent binding is probably the reason why practically no BMP-2 was released from the PDA coatings without the use of CS-TPP-NP and might also contribute to the fact that only about one third was released with the use of CS-TPP-NP in our experiments.

X-ray photoelectron spectroscopic measurements revealed that alginate and CS layers mix during loading, that there is no clear separation of the individual polyelectrolyte layers and that the TPP is almost completely washed out of the forming matrix (Sydow, de Cassan, et al., 2019). The coating resulting from the use of CS-TPP-

NP on the CS-g-PCL-Alg variants must, therefore, be considered as a mixed alginate-chitosan matrix. Because of the incorporation of BMP-2 during the layer build-up and the complete release, it can be assumed that BMP-2 is largely incorporated into the interior of this matrix and is released primarily via matrix degradation. This hypothesis is supported by the fast layer degradation during the first few days of incubation in PBS, shown by Sydow, Aniol, Hadler, and Menzel (2019), which correlates well with the fast BMP-2 release shown in this study.

On the PDA and plasma variants, however, an alginate-free CS matrix is coated onto the surface. Based on similar release patterns of the CS-g-PCL-Alg and plasma variants (Figure 8), it can be assumed that both matrices exhibited a similar degradation behavior. As a result of the proportion of about two-thirds of BMP-2 on the PDA variants that were not released under the tested conditions there still seemed to be some binding of BMP-2 directly to the modified surface. Nevertheless, the PDA variants might be very promising for *in vivo* use despite the incomplete release *in vitro* as the release *in vivo* might be higher because of the influence of bleeding, wound healing, enzymatic and immunological processes after implantation. *In vivo*, there might also be an interaction between stem cells whose surface receptors come into direct contact with unreleased BMP-2 on the PCL fibers (Lee et al., 2018; Pohl, Boergemann, Schwaerzer, Knaus, & Cavalcanti-Adam, 2012).

A complete release from the CS-g-PCL-Alg systems is ensured by the fact that the alginate surface itself can degrade, revealing the BMP-2 repelling cationic CS-g-PCL coating. In contrast, the PDA variants offered a surface to which the BMP-2 might irreversibly be bound after the complete dissolution of the CS matrix.

Because of the low solubility of BMP-2 in physiologic media, a valid quantification of released BMP-2 by ELISA or other biological assays can only be ensured with limitations, which is why Cy3-BMP-2 was used in the present study. Most interfering effects on quantification can also be effectively avoided by a radioiodine labeling of BMP-2. Corresponding studies have revealed a complete BMP-2 release associated with hydrogel matrix degradation. Yamamoto et al. (2003) showed complete release of ¹²⁵I-labeled BMP-2 from a degradable gelatin hydrogel *in vivo*, while Patel et al. (2015) reported that the *in vitro* release of ¹²⁵I-labeled BMP-2 strongly depended on the degradability of gelatin microspheres, reaching from 32% cumulative release for non-degradable microspheres to 100% for completely degradable ones. Liu et al. (2018) revealed that more than 50% percent of loaded ¹³¹I-labeled BMP-2 remained entrapped after 5 weeks inside a calcium phosphate coating of titanium-based implants *in vivo* while surface adsorbed BMP-2 was completely depleted after 2 weeks. *In vitro*, however, only 40% of the surface-adsorbed BMP-2 was released from the same coatings after 5 weeks.

In this study, a complete BMP-2 release could be achieved by incorporating the protein into a chitosan matrix on plasma or CS-g-PCL-Alg fiber mat variants. In contrast, the direct binding of BMP-2 to non-degradable surfaces led to an incomplete release *in vitro*. Unmodified PCL showed a high BMP-2 loading without CS-TPP-NP but only about one-third of the bound portion was released *in vitro*,

which was probably mainly a result of the poor wetting of the fiber mat samples. Unmodified PCL is not biocompatible *in vivo* and leads to encapsulation into fibrous tissue (Gniesmer et al., 2019). For this reason and due to the poor wettability, unmodified PCL fiber mats are not suitable for the use as parenteral drug delivery systems.

All CS-TPP-NP-coated systems showed a similar release pattern with a strong burst release and a subsequent sustained release (Figure 8). The sustained release was apparently not complete after the observation periods of 50 and 70 days. The release rate during the seventh week of the release study, however, was only in the range of ~12–21 pg/cm²/day, which may not be sufficient for a physiological effect. The minimum release rate required to maintain a BMP-2 effect is still an open field of research. BMP-2 doses ranging from 100 ng to several milligrams in combination with various implant prototypes have proven to be effective *in vivo* (Agrawal & Sinha, 2017; Begam, Nandi, Kundu, & Chanda, 2017; Prabhath et al., 2018). However, a steep dose-response relationship was found for BMP-2 loaded to collagen-based scaffolds in the range of 2–15 µg in the rat ectopic model (Porter, Rathore, Rouse, & Denton, 2004; Uludag et al., 2000). In comparison, 50 mg of our PCL fiber scaffold would contain a dose in the range of 5–15 µg BMP-2, depending on the surface modification, the loading duration, and the specific surface area resulting from the fiber diameter.

4.3 | Loading duration and binding efficiency

The loading per cm² fiber mat surface after 15 min did not seem to be influenced by the varying concentration decrease in the loading solution, as shown by the comparison of L1 and L2 (Table 1, Figure 4a,b). The BMP-2 concentration in the loading solution, therefore, seems to not significantly limit the binding rates in the range of 2.8–10.2 µg/ml. Presumably, this concentration range was well above the equilibrium concentration that would occur as a result of complete surface saturation. With the same loading duration, the bound quantity, therefore, only depended on the used fiber mat surface.

The loading experiments showed that loading efficiency could be slightly increased by extending the incubation time. When loading CS-g-PCL-Alg fiber mats, however, too long incubation may lead to the dissolution of the already formed alginate layer. In the case of loading experiment L2, the loading efficiency could be increased from 33 to 48% by doubling the incubation time to 30 min, which did not have any noticeable influence on the release kinetics (Figure 4d).

Hettiaratchi et al. investigated the binding of BMP-2 to heparin microparticles and found that about 87% of the total amount of BMP-2 was bound to the microparticles after 30 min, which increased to 91% after 90 min and reached a maximum after 4 hr (Hettiaratchi et al., 2017). Even though loading experiments of dispersed heparin particles have only limited comparability to our experiments, it is to be expected that the time until reaching equilibrium is rather even longer when loading fiber mats, because of the longer diffusion paths inside the loading solution. On the other hand, Hettiaratchi et al. used at least 10 times lower BMP-2 concentrations, which might have had a

limiting effect on the loading kinetics. Similarly, high loading efficiency of 87% was also measured by Chen et al. when loading dextran micro-particles with ^{125}I -labeled BMP-2 (Chen et al., 2006).

Kang et al. investigated the binding of a BMP-2-GFP construct to hydroxyapatite bone grafts at different temperatures and found that almost complete loading occurred after about 30 min at 37°C and after about 60 min at 20°C (Kang, Lee, & Jang, 2015). As our loading tests were all carried out at 26°C, the maximum loading found for the PDA variants and the plasma variants at ~20–40 min fits in well with these results. However, the loading could probably be accelerated by increasing the temperature.

5 | CONCLUSION

This study demonstrates that BMP-2 loading on surface-modified PCL fiber mats strongly depends on the fiber diameter and resulting available surface area as well as on the type of surface modification. Using a surface modification leading to strong BMP-2 binding did not necessarily result in a high BMP-2 release. On the contrary, a strong connection to PDA-surface modifications of PCL or direct binding to hydrophobic unmodified PCL surfaces without the use of CS-TPP-NP led to a very low BMP-2 release *in vitro*. The use of CS-TPP-NP led to an increased protein loading on all surface modifications and allowed a longer-lasting and more complete release compared to the direct superficial binding. Apparently, BMP-2 was incorporated into the formed chitosan nanogel coating upon loading with CS-TPP-NP. However, with a CS coating as applied here, the portion of protein released in a sustained manner was still quite small. Although large molecules such as proteins can be effectively retained in CS matrices (George & Abraham, 2006), CS's ability to control the release of embedded substances is limited by its rapid dissolution rate.

ACKNOWLEDGMENTS

We thank the Deutsche Forschungsgemeinschaft for funding within the research unit "Gradierte Implantate" (FOR 2180), the Ministry of Science and Culture (MWK) of Lower Saxony, Germany, for the financial support within the Smart BioTecs alliance, Alexander Becker and colleagues at the Institute for Multiphase Processes, Leibniz Universität Hannover, for the supply of electrospun batch fiber mats and Stefanie Dirksen-Thedens for her experimental support. Open access funding enabled and organized by Projekt DEAL.

ORCID

Julius Sundermann  <https://orcid.org/0000-0001-8731-0770>

Robert Hänsch  <https://orcid.org/0000-0003-1310-8419>

Ursula Rinas  <https://orcid.org/0000-0003-4940-5749>

Henning Menzel  <https://orcid.org/0000-0002-4915-7311>

REFERENCES

Abarrategi, A., García-Cantalejo, J., Moreno-Vicente, C., Civantos, A., Ramos, V., Casado, J. V. S., ... López-Lacomba, J. L. (2009). Gene

- expression profile on chitosan/rhBMP-2 films: A novel osteoinductive coating for implantable materials. *Acta Biomaterialia*, 5, 2633–2646.
- Agrawal, V., & Sinha, M. (2017). A review on carrier systems for bone morphogenetic protein-2. *Journal of Biomedical Materials Research Part B: Applied Biomaterials*, 105, 904–925.
- Amini, A. R., Laurencin, C. T., & Nukavarapu, S. P. (2012). Bone tissue engineering: Recent advances and challenges. *Critical Reviews in Biomedical Engineering*, 40, 363–408.
- Begam, H., Nandi, S. K., Kundu, B., & Chanda, A. (2017). Strategies for delivering bone morphogenetic protein for bone healing. *Materials Science & Engineering C, Materials for Biological Applications*, 70, 856–869.
- Boudou, T., Crouzier, T., Ren, K., Blin, G., & Picart, C. (2010). Multiple functionalities of polyelectrolyte multilayer films: New biomedical applications. *Advanced Materials*, 22, 441–467.
- Cao, L., Wang, J., Hou, J., Xing, W., & Liu, C. (2014). Vascularization and bone regeneration in a critical sized defect using 2-N,6-O-sulfated chitosan nanoparticles incorporating BMP-2. *Biomaterials*, 35, 684–698.
- Chen, F.-m., Z-f, W., Sun, H.-h., Wu, H., S-n, X., Q-t, W., ... Jin, Y. (2006). Release of bioactive BMP from dextran-derived microspheres: A novel delivery concept. *International Journal of Pharmaceutics*, 307, 23–32.
- Cho, H.-J., Perikamana, S. K. M., Lee, J.-h., Lee, J., Lee, K.-M., Shin, C. S., & Shin, H. (2014). Effective immobilization of BMP-2 mediated by polydopamine coating on biodegradable nanofibers for enhanced *in vivo* bone formation. *ACS Applied Materials & Interfaces*, 6, 11225–11235.
- Costa, R. R., & Mano, J. F. (2014). Polyelectrolyte multilayered assemblies in biomedical technologies. *Chemical Society Reviews*, 43, 3453–3479.
- de Cassan, D., Sydow, S., Schmidt, N., Behrens, P., Roger, Y., Hoffmann, A., ... Menzel, H. (2018). Attachment of nanoparticulate drug-release systems on poly(ϵ -caprolactone) nanofibers via a graftpolymer as interlayer. *Colloid Surface B*, 163, 309–320.
- Desmet, T., Morent, R., de Geyter, N., Leys, C., Schacht, E., & Dubruel, P. (2009). Nonthermal plasma technology as a versatile strategy for polymeric biomaterials surface modification: A review. *Biomacromolecules*, 10, 2351–2378.
- Drotleff, S., Lungwitz, U., Breunig, M., Dennis, A., Blunk, T., Tessmar, J., & Göpferich, A. (2004). Biomimetic polymers in pharmaceutical and biomedical sciences. *European Journal of Pharmaceutics and Biopharmaceutics*, 58, 385–407.
- Freier, T., Koh, H. S., Kazazian, K., & Shoichet, M. S. (2005). Controlling cell adhesion and degradation of chitosan films by N-acetylation. *Biomaterials*, 26, 5872–5878.
- Gan, Q., Wang, T., Cochrane, C., & McCarron, P. (2005). Modulation of surface charge, particle size and morphological properties of chitosan-TPP nanoparticles intended for gene delivery. *Colloid Surface B*, 44, 65–73.
- George, M., & Abraham, T. E. (2006). Polyionic hydrocolloids for the intestinal delivery of protein drugs: Alginate and chitosan—A review. *Journal of Controlled Release*, 114, 1–14.
- Gniesmer, S., Brehm, R., Hoffmann, A., de Cassan, D., Menzel, H., Hoheisel, A.-L., ... Kampmann, A. (2019). *In vivo* analysis of vascularization and biocompatibility of electrospun polycaprolactone fibre mats in the rat femur chamber. *Journal of Tissue Engineering and Regenerative Medicine*, 13, 1190–1202.
- Hettiaratchi, M. H., Chou, C., Servies, N., Smeekens, J. M., Cheng, A., Esancy, C., ... Krishnan, L. (2017). Competitive protein binding influences heparin-based modulation of spatial growth factor delivery for bone regeneration. *Tissue Engineering. Part A*, 23, 683–695.
- Jewell, C. M., & Lynn, D. M. (2008). Multilayered polyelectrolyte assemblies as platforms for the delivery of DNA and other nucleic acid-based therapeutics. *Advanced Drug Delivery Reviews*, 60, 979–999.
- Kang, W., Lee, D.-S., & Jang, J.-H. (2015). Evaluation of sustained BMP-2 release profiles using a novel fluorescence-based retention assay. *PLoS One*, 10, e0123402.

- Korchynskiy, O., & ten Dijke, P. (2002). Identification and functional characterization of distinct critically important bone morphogenetic protein-specific response elements in the *Id1* promoter. *The Journal of Biological Chemistry*, 277, 4883–4891.
- Lee, J. S., Lee, J.-C., & Heo, J. S. (2018). Polydopamine-assisted BMP-2 immobilization on titanium surface enhances the osteogenic potential of periodontal ligament stem cells via integrin-mediated cell-matrix adhesion. *Journal of Cell Communication and Signaling*, 12, 661–672.
- Lee, K.-W., Lee, J.-S., Kim, Y.-S., Shim, Y.-B., Jang, J.-W., & Lee, K.-I. (2016). Effective healing of chronic rotator cuff injury using recombinant bone morphogenetic protein-2 coated dermal patch in vivo. *Journal of Biomedical Materials Research Part B: Applied Biomaterials*, 105, 1–7.
- Liu, Y., Schouten, C., Boerman, O., Wu, G., Jansen, J. A., & Hunziker, E. B. (2018). The kinetics and mechanism of bone morphogenetic protein 2 release from calcium phosphate-based implant-coatings. *Journal of Biomedical Materials Research. Part A*, 106, 2363–2371.
- Lochmann, A., Nitzsche, H., von Einem, S., Schwarz, E., & Mäder, K. (2010). The influence of covalently linked and free polyethylene glycol on the structural and release properties of rhBMP-2 loaded microspheres. *Journal of Controlled Release*, 147, 92–100.
- Longo, U. G., Lamberti, A., Rizzello, G., Maffulli, N., & Denaro, V. (2012). Synthetic augmentation in massive rotator cuff tears. *Medicine and Sport Science*, 57, 168–177.
- Lorenz, C., Hoffmann, A., Gross, G., Windhagen, H., Dellinger, P., Möhwald, K., ... Menzel, H. (2011). Coating of titanium implant materials with thin polymeric films for binding the signaling protein BMP2. *Macromolecular Bioscience*, 11, 234–244.
- Marquetti, I., & Desai, S. (2018). Molecular modeling the adsorption behavior of bone morphogenetic protein-2 on hydrophobic and hydrophilic substrates. *Chemical Physics Letters*, 706, 285–294.
- Martino, M. M., Tortelli, F., Mochizuki, M., Traub, S., Ben-David, D., Kuhn, G. A., ... Hubbell, J. A. (2011). Engineering the growth factor microenvironment with fibronectin domains to promote wound and bone tissue healing. *Science Translational Medicine*, 3, 100ra89.
- Olthof, M. G. L., Kempen, D. H. R., Liu, X., Dadsetan, M., Tryfonidou, M. A., Yaszemski, M. J., ... Lu, L. (2018). Bone morphogenetic protein-2 release profile modulates bone formation in phosphorylated hydrogel. *Journal of Tissue Engineering and Regenerative Medicine*, 12, 1339–1351.
- Patel, J. J., Modes, J. E., Flanagan, C. L., Krebsbach, P. H., Edwards, S. P., & Hollister, S. J. (2015). Dual delivery of EPO and BMP2 from a novel modular poly-epsilon-caprolactone construct to increase the bone formation in prefabricated bone flaps. *Tissue Engineering. Part C, Methods*, 21, 889–897.
- Pohl, T. L. M., Boergermann, J. H., Schwaerzer, G. K., Knaus, P., & Cavalcanti-Adam, E. A. (2012). Surface immobilization of bone morphogenetic protein 2 via a self-assembled monolayer formation induces cell differentiation. *Acta Biomaterialia*, 8, 772–780.
- Polycaprolactone. (2018). MSDS No. 440744 Version 6.1 [online]; Sigma-Aldrich: St. Louis, MO. Retrieved from <https://www.sigmaaldrich.com/MSDS/MSDS/DisplayMSDSPage.do?country=DE&language=EN-generic&productNumber=440744&brand=ALDRICH&PageToGoToURL=https%3A%2F%2Fwww.sigmaaldrich.com%2Fcatalog%2Fsearch%3Fterm%3Dpoly%20caprolactone%26interface%3DAI%26N%3D0%26mode%3Dmatch%2520partialmax%26lang%3Dde%26region%3DDE%26focus%3Dproduct>. Accessed 30 August 2019.
- Porter, T. J., Rathore, S., Rouse, J., & Denton, M. (2004). Biomolecules in tissue engineered medical products (TEMPs): A case study of recombinant human bone morphogenetic protein-2 (rhBMP-2). *Journal of ASTM International*, 1, 1–24.
- Poth, N., Seiffart, V., Gross, G., Menzel, H., & Dempwolf, W. (2015). Biodegradable chitosan nanoparticle coatings on titanium for the delivery of BMP-2. *Biomolecules*, 5, 3–19.
- Prabhath, A., Vernekar, V. N., Sanchez, E., & Laurencin, C. T. (2018). Growth factor delivery strategies for rotator cuff repair and regeneration. *International Journal of Pharmaceutics*, 544, 358–371.
- Qiang, W., Li, W., Li, X., Chen, X., & Xu, D. (2014). Bioinspired polydopamine nanospheres: A superquencher for fluorescence sensing of biomolecules. *Chemical Science*, 5, 3018–3024.
- Quaas, B., Burmeister, L., Li, Z., Nitz, M., Hoffmann, A., & Rinas, U. (2018). Properties of dimeric, disulfide-linked rhBMP-2 recovered from *E. coli* derived inclusion bodies by mild extraction or chaotropic solubilization and subsequent refolding. *Process Biochemistry*, 67, 80–87.
- Quaas, B., Burmeister, L., Li, Z., Satalov, A., Behrens, P., Hoffmann, A., & Rinas, U. (2019). Stability and biological activity of *E. coli* derived soluble and precipitated bone morphogenetic protein-2. *Pharmaceutical Research*, 36, 184.
- Quinlan, E., López-Noriega, A., Thompson, E., Kelly, H. M., Cryan, S. A., & O'Brien, F. J. (2015). Development of collagen-hydroxyapatite scaffolds incorporating PLGA and alginate microparticles for the controlled delivery of rhBMP-2 for bone tissue engineering. *Journal of Controlled Release*, 198, 71–79.
- Rabe, M., Verdes, D., & Seeger, S. (2011). Understanding protein adsorption phenomena at solid surfaces. *Advances in Colloid and Interface Science*, 162, 87–106.
- Ruhé, P. Q., Boerman, O. C., Russel, F. G. M., Mikos, A. G., Spauwen, P. H. M., & Jansen, J. A. (2006). In vivo release of rhBMP-2 loaded porous calcium phosphate cement pretreated with albumin. *Journal of Materials Science. Materials in Medicine*, 17, 919–927.
- Ruppert, R., Hoffmann, E., & Sebald, W. (1996). Human bone morphogenetic protein 2 contains a heparin-binding site which modifies its biological activity. *European Journal of Biochemistry*, 237, 295–302.
- Ryu, J. H., Messersmith, P. B., & Lee, H. (2018). Polydopamine surface chemistry: A decade of discovery. *ACS Applied Materials & Interfaces*, 10, 7523–7540.
- Shields, L. B. E., Raque, G. H., Glassman, S. D., Campbell, M., Vitaz, T., Harpring, J., & Shields, C. B. (2006). Adverse effects associated with high-dose recombinant human bone morphogenetic protein-2 use in anterior cervical spine fusion. *Spine*, 31, 542–547.
- Strobel, C., Bormann, N., Kadow-Romacker, A., Schmidmaier, G., & Wildemann, B. (2011). Sequential release kinetics of two (gentamicin and BMP-2) or three (gentamicin, IGF-I and BMP-2) substances from a one-component polymeric coating on implants. *Journal of Controlled Release*, 156, 37–45.
- Sydow, S., Aniol, A., Hadler, C., & Menzel, H. (2019). Chitosan-azide nanoparticle coating as a degradation barrier in multilayered polyelectrolyte drug delivery systems. *Biomolecules*, 9, 573.
- Sydow, S., de Cassan, D., Hänsch, R., Gengenbach, T. R., Easton, C. D., Thissen, H., & Menzel, H. (2019). Layer-by-layer deposition of chitosan nanoparticles as drug-release coatings for PCL nanofibers. *Biomaterials Science*, 7, 233–246.
- Uludag, H., D'Augusta, D., Golden, J., Timony, G., Li, J., Riedel, R., & Wozney, J. M. (2000). Implantation of recombinant human bone morphogenetic proteins with biomaterial carriers: A correlation between protein pharmacokinetics and osteoinduction in the rat ectopic model. *Journal of Biomedical Materials Research*, 50, 227–238.
- Uludag, H., D'Augusta, D., Palmer, R., Timony, G., & Wozney, J. M. (1999). Characterization of rhBMP-2 pharmacokinetics implanted with biomaterial carriers in the rat ectopic model. *Journal of Biomedical Materials Research*, 46, 193–202.
- Utesch, T., Daminelli, G., & Mroginski, M. A. (2011). Molecular dynamics simulations of the adsorption of bone morphogenetic protein-2 on surfaces with medical relevance. *Langmuir*, 27, 13144–13153.
- Vogler, E. A. (1998). Structure and reactivity of water at biomaterial surfaces. *Advances in Colloid and Interface Science*, 74, 69–117.

- Vroman, L., & Adams, A. L. (1969). Identification of rapid changes at plasma-solid interfaces. *Journal of Biomedical Materials Research*, 3, 43–67.
- Wang, Q., Wang, M., Li, P., Wang, K., Fang, L., Ren, F., ... Lu, X. (2019). The interaction of chitosan and BMP-2 tuned by deacetylation degree and pH value. *Journal of Biomedical Materials Research. Part A*, 107, 769–779.
- Xia, Y.-J., Xia, H., Chen, L., Ying, Q.-S., Yu, X., Li, L.-H., ... Zhang, Y. (2018). Efficient delivery of recombinant human bone morphogenetic protein (rhBMP-2) with dextran sulfate-chitosan microspheres. *Experimental and Therapeutic Medicine*, 15, 3265–3272.
- Yamamoto, M., Takahashi, Y., & Tabata, Y. (2003). Controlled release by biodegradable hydrogels enhances the ectopic bone formation of bone morphogenetic protein. *Biomaterials*, 24, 4375–4383.
- Zhao, X., Han, Y., Li, J., Cai, B., Gao, H., Feng, W., ... Li, D. (2017). BMP-2 immobilized PLGA/hydroxyapatite fibrous scaffold via polydopamine

stimulates osteoblast growth. *Materials Science & Engineering. C, Materials for Biological Applications*, 78, 658–666.

SUPPORTING INFORMATION

Additional supporting information may be found online in the Supporting Information section at the end of this article.

How to cite this article: Sundermann J, Oehmichen S, Sydow S, et al. Varying the sustained release of BMP-2 from chitosan nanogel-functionalized polycaprolactone fiber mats by different polycaprolactone surface modifications. *J Biomed Mater Res*. 2021;109:600–614. <https://doi.org/10.1002/jbm.a.37045>